Ocean Model Diagnosis of Interannual Coevolving SST Variability in the South Indian and South Atlantic Oceans

J. C. HERMES AND C. J. C. REASON

Department of Oceanography, University of Cape Town, Rondebosch, South Africa

(Manuscript received 27 February 2004, in final form 4 October 2004)

ABSTRACT

A global ocean model (ORCA2) forced with 50 yr of NCEP–NCAR reanalysis winds and heat fluxes has been used to investigate the evolution and forcing of interannual dipolelike sea surface temperature (SST) variability in the South Indian and South Atlantic Oceans. Although such patterns may also exist at times in only one of these basins and not the other, only events where there are coherent signals in both basins during the austral summer have been chosen for study in this paper. A positive (negative) event occurs when there is a significant warm (cool) SST anomaly evident in the southwest of both the South Indian and South Atlantic Oceans and a cool (warm) anomaly in the eastern subtropics.

The large-scale forcing of these events appears to consist of a coherent modulation of the wavenumber-3 or -4 pattern in the Southern Hemisphere atmospheric circulation such that the semipermanent subtropical anticyclone in each basin is shifted from its summer mean position and its strength is modulated. A relationship to the Antarctic Oscillation is also apparent, and seems to strengthen after the mid-1970s. The modulated subtropical anticyclones lead to changes in the tropical easterlies and midlatitude westerlies in the South Atlantic and South Indian Oceans that result in anomalies in latent heat fluxes, upwelling, and Ekman heat transports, all of which contribute to the SST variability. In addition, there are significant modulations to the strong Rossby wave signals in the South Indian Ocean. The results of this study confirm the ability of the ORCA2 model to represent these dipole patterns and indicate connections between large-scale modulations of the Southern Hemisphere midlatitude atmospheric circulation and coevolving SST variability in the South Atlantic and South Indian Oceans.

1. Introduction

A number of investigations into the links between sea surface temperature (SST) anomalies in the South Indian Ocean and southern African climate variability have been carried out (Walker and Mey 1988; Walker 1990; Mason 1995; Reason 1999; Reason and Mulenga 1999; Reason 2002). A particular phenomenon that has more recently provoked interest is the so-called subtropical Indian Ocean dipole (SIOD) pattern, which is evident in South Indian Ocean SST anomalies (Behera and Yamagata 2001; Reason 2001). A similar dipolelike pattern in SST may also be evident in the South Atlantic Ocean (Venegas et al. 1997; Fauchereau et al. 2003).

The South Indian Ocean dipole pattern was derived by Behera and Yamagata (2001, hereafter BY01) using simple EOFs of observational SST data. These authors defined a positive event to consist of negative SST anomalies in the southeastern Indian Ocean (off the coast of Western Australia), with the largest anomalies covering the area 29°–10°S, 85°–105°E and positive SST anomalies in the southwestern Indian Ocean, at 42°–30°S, 50°–80°E. The reverse is seen during a negative event. BY01 and Suzuki et al. (2004) linked the SIOD to austral summer/autumn because the depth of the surface mixed layer is shallowest then; hence, the wind-driven latent heat flux anomalies, which are believed to be the major factor in the anomalous SST evolution, influences the SST most efficiently at this time of year.

Fauchereau et al. (2003, hereafter F03) also used observational data but focused more on the covariability in austral summer SST between the South Indian and South Atlantic Oceans. Similar to F03, this study also considers the interannual variability of both the South Atlantic Ocean and the South Indian Ocean and examines cases where both basins show a similar summer dipolelike pattern. F03 defined the South Atlantic

Corresponding author address: Dr. J. C. Hermes, Department of Oceanography, University of Cape Town, Private Bag, Rondebosch 7701, South Africa.
E-mail:jhermes@ocean.uct.ac.za

warm and cool poles as western (40°–30°S, 35°–15°W) and eastern (30°–18°S, 15°W–15°E) during a positive event; with the reverse polarity defining a negative event. The study of F03 did not consider the negative events or the evolution of the cool pole during the positive events. This study extends the previous work of F03 by looking at both negative and positive events, thereby considering the potential nonlinearity between them, and by using an ocean general circulation model (OGCM) to investigate the ocean processes that may contribute to their evolution. The model used is the ORCA2 OGCM (Rodgers et al. 2003) forced by over 50 yr of NCEP–NCAR reanalyses (Kalnay et al. 1996). The role that large-scale atmospheric forcing may play during the evolution of the events in both oceans is examined by means of the NCEP–NCAR reanalyses.

In addition to a need to better understand the evolution of these patterns in the South Atlantic and South Indian Oceans, an important motivation for studying them is because of the substantial evidence of their influence on regional rainfall. Both observations (BY01) and atmospheric models (Reason 2001, 2002) strongly indicate that the South Indian Ocean SST anomalies may affect rainfall over southern Africa. On the basis of these experiments, Reason (2002) suggested that the response over southeastern Africa is stronger when the western pole is closer to the subcontinent and that the response over the subtropical (tropical) landmass appears to be insensitive (sensitive) to the eastern pole. Qian et al. (2002) presented evidence that these events may also impact on rainfall in northern Australia and southern Asia. Although these studies have indicated that these events may influence rainfall variability over the neighboring landmasses, a better understanding of their evolution and mechanisms is clearly needed, if the goal of more accurate SST prediction is to be realized. As a step in that direction, the OGCM analyses presented herein shed further light on the important forcing mechanisms and potential feedbacks.

In the next section, a description of the OGCM together with validation against observations will be given. Section 3 demonstrates the evolution of the warm and cold poles during both positive and negative years. The large-scale forcing of the events and the ocean response to it is discussed in section 4. The final section contains the conclusions.

2. Model description and validation

The model results were obtained from the ocean general circulation model, Ocean Parallelisé (OPA; Madec et al. 1998), and the configuration used is ORCA2 (Rodgers et al. 2003). Overall, the domain, which extends from 78°S to 90°N, has a zonal resolution of 2° and the meridional resolution ranges from 0.5° at the equator to 2° × cosine (latitude) poleward of 20° in either hemisphere. In the vertical, there are 30 layers from the surface to 5000-m depth, the first 20 of which lie in the upper 500 m. The model has two poles in the Northern Hemisphere and one centered over Antarctica. It is coupled with a sea ice model, representing both dynamic and thermodynamic processes (Morales Maqueda 1995; Rodgers et al. 2003; Fichefet and Morales Maqueda 1997). The bottom topography is derived from Smith and Sandwell (1997), as are the coastlines.

TABLE 1. Nomenclature of dipole years and months.

Yr	Description	Model month	Calendar month
Onset yr	Yr preceding and leading up to an event	1–15	1–12
Event yr	Yr when anomalies were max	16–30	13–24
Subsequent yr	Yr following the event	31–45	25–36

The model was initialized with Levitus et al. (1998) temperature and salinity values and spun up for 200 yr, with a restoring boundary condition on surface salinity (2-month time scale). It was then run for a further 52 yr, using NCEP–NCAR reanalysis and heat fluxes for the 1948–99 period. A salinity flux correction for this period was imposed by applying the annual mean fluxes from the last 50 yr to the interannually varying NCEP–NCAR runs. The surface temperature boundary conditions include a bulk mixed layer that receives air temperature, air humidity, total cloudiness, surface pressure, and surface wind speed from NCEP–NCAR data from 1948 to 1999. From this data, surface heat fluxes are calculated.

Model output is produced every 24.33 days as average flow fields, thus there are 15 "months" to a model year, as a result of the time step chosen (Table 1). [Further details of the model are given in Rodgers et al. (2003), Madec et al. (1998), and online at http://www.lodyc.jussieu.fr/opa.] The validity of this run of ORCA2 has not been previously published and so model SST are compared below with the Met Office Global Sea Ice and Sea Surface Temperature (GISST) 2.3 dataset (Rayner et al. 1996) for the years 1948–99 (Figs. 1a–e). Both the ORCA2 and the GISST 2.3 datasets have been detrended by removing the best-fit linear trend.

Time series of spatially averaged SST over the warm and cold poles compare favorably when derived with

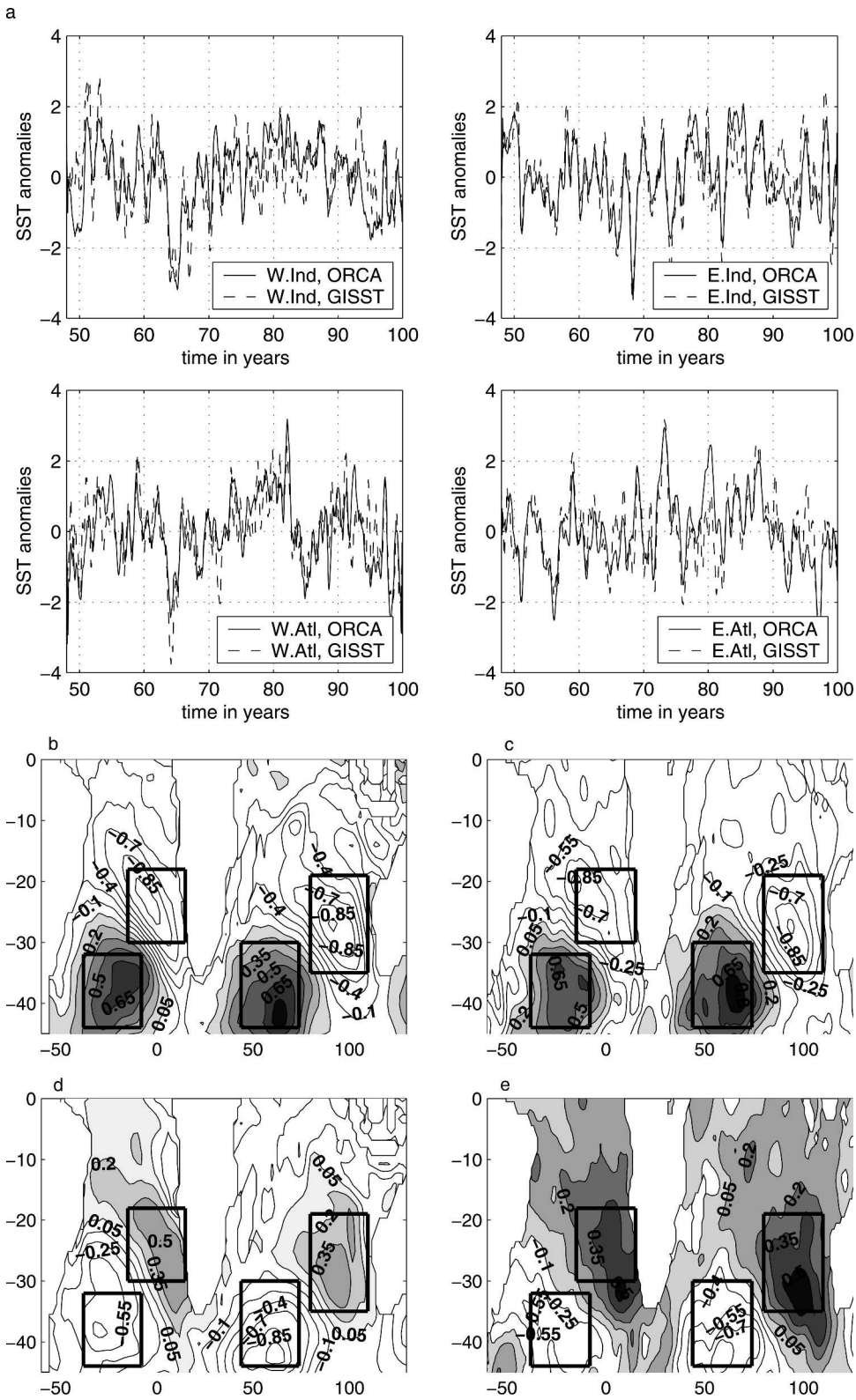

FIG. 1. (a) Time series of SST anomalies averaged over the western Indian Ocean (30°–44°S, 44°–74°E), the eastern Indian Ocean (19°–35°S, 80°–110°E), the western Atlantic Ocean (32°–44°S, 38°–8°W), and the eastern Atlantic Ocean (18°–30°S, 15°W–15°E) using the Met Office GISST2.3 dataset (dashed) and ORCA2 data (solid). (b) ORCA2 SST anomalies for JFM of the positive event. Contour interval is 0.15°C, positive (negative) values are shaded gray (white). (c) Same as for (b), except using the Met Office GISST2.3 data. (d), (e) Same as (b), (c), respectively, but for the negative event.

ORCA2 and GISST 2.3 data (overall correlation 0.9; Fig. 1a). A similar correspondence of the spatial patterns for the austral summer [January–February–March (JFM)] composites for the positive and negative event years (Figs. 1b–e) is evident. Austral summer composites were used as the dipolelike pattern is at its most prominent then, and there is little variability from one month to the next. Although the spatial patterns are very similar, the ORCA2 anomalies appear smoother, possibly due to the slightly coarser resolution of the model relative to the observations and diffusion applied to ensure stability of the model integration. The spatial patterns of the anomalies are also comparable to those derived by BY01 and F03 (although the center of the anomalies in this study extend farther into the midlatitudes).

Composites are used in order to highlight the main features of the dipole events and to reduce the noise of individual cases. The positive events were chosen by visual examination of the raw ORCA2 model dataset such that a coherent warm (cold) SST anomaly is found during austral summer on the western (eastern) side of the subtropical/midlatitude basin of both oceans with a southeast–northwest orientation in each case (Figs. 1b–e). Negative events are defined such that the warm (cold) SST anomaly is on the eastern (western) side of each basin. As a result, positive events are defined as 1951, 1962, 1976, 1981, 1982, 1990, 1997, and 1999 and negative events as 1949, 1950, 1957, 1964, 1972, 1975, and 1988. Since the events occur during austral summer, the years defined refer to JFM. Note that the same set of years result if GISST 2.3 SST data are used. Singular value decomposition was also performed between the sea surface temperature and the sea level pressure in the South Indian and South Atlantic Oceans. The specific years listed above are consistent with the resulting singular value decomposition (SVD) expansion coefficient time series. Table 2 lists all of the strongest dipole events that occur during the summer months (in both model and GISST 2.3 data), of 1949–99 in each ocean. The coevolving events used in the composites in this study are shown in bold.

Since only those years where a dipole occurred in both oceans have been included in these composites, certain years defined by BY01 for the South Indian Ocean only have been excluded. About 70% of the strong events occur in both oceans, suggesting that these events may possibly be linked by large-scale near-hemispheric forcing. In addition, we consider events occurring back to 1949 whereas BY01 focused on data after 1958. An example of a South Indian Ocean dipole event defined by BY01 but not herein is 1968, which was a strong "dipole" year in the South Indian Ocean, but there was no coinciding dipole pattern in the South Atlantic. Another example is 1974, when there was only a very weak dipole pattern visible in the South Atlantic for 1 month. The BY01 positive event of 1993 was also excluded, as no dipole pattern was apparent in the South Atlantic Ocean and only a weak dipole occurred in the South Indian Ocean. The years chosen here also vary from those used by F03 as their study chose years based on the size of the summer positive anomalies in the southwest Indian Ocean and the southwest Atlantic Ocean. Thus, the positive composite derived here consists of five of the same years, but excludes 1953, 1959, and 1992, when there was a strong positive anomaly in the southwest, but not an obvious negative anomaly in the southeast of each basin. Years included in this study but not in that of F03 are 1990, 1997, and 1999 as the positive anomalies alone were not as strong as other years, but there was a robust dipole pattern. However, it should be noted that there is some variation in the position of the SST anomalies between events in each composite and, because of differences in the years used in the composites, it is expected that the center of the anomalies will differ slightly from those defined by BY01 and F03.

TABLE 2. List of years when a positive/negative dipole event occurs in the South Indian and South Atlantic Oceans. The coevolving events used in the composites in this study are shown in bold.

Positive dipole		Negative dipole	
South Atlantic	South Indian	South Atlantic	South Indian
1951	**1951**	**1949**	**1949**
1955	1953	**1950**	**1950**
1962	1968	**1957**	**1957**
1970	**1962**	**1964**	1958
1976	1974	1969	**1964**
1979	**1976**	**1972**	**1972**
1981	**1981**	1973	1970
1982	**1982**	**1975**	**1975**
1990	**1990**	1985	1983
1997	1993	**1988**	**1988**
1999	**1997**	1993	1995
	1999		1998

3. Evolution of the SST dipolelike pattern

To be considered a true dipole, both poles should form at the same time, with a similar intensity and spatial distribution. To investigate this, the normalized model SST anomaly in the east of each ocean basin has been plotted against that in the west for the onset, event, and subsequent years for both positive (Fig. 2a) and negative (Fig. 2b) composite events. Similar figures

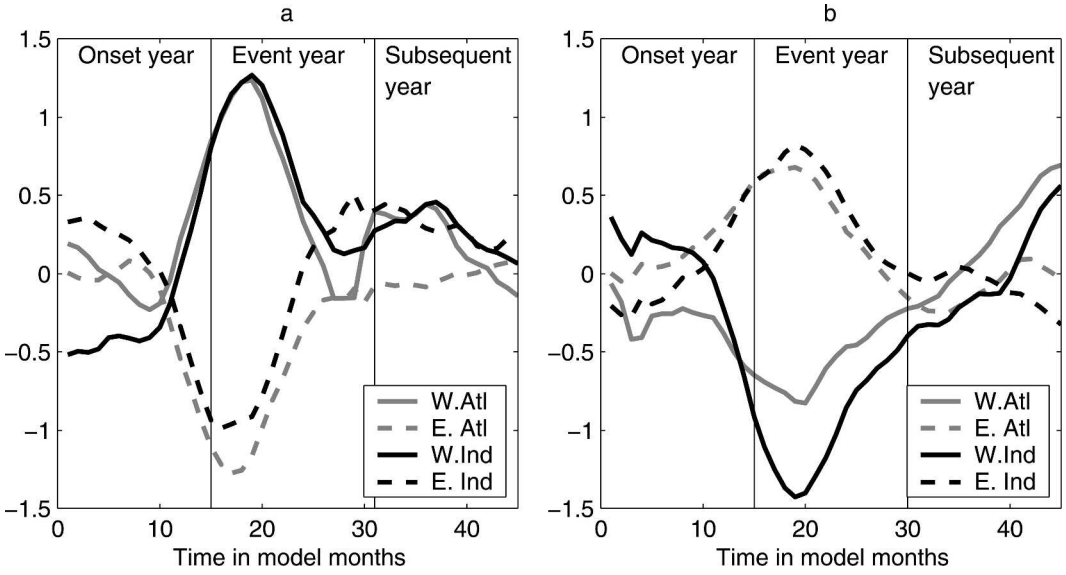

FIG. 2. (a) ORCA2 SST anomalies for the western (black solid) and eastern (black dashed) Indian Ocean and the western (gray solid) and eastern (gray dashed) Atlantic Ocean, during the onset and event years of the positive event. (b) Same as for (a), but for the negative event.

were produced for the GISST dataset (not shown) and compare favorably. Figure 2 suggests that this phenomenon does indeed evolve as a dipole. For both the positive and negative events, the model SST anomalies can reach up to 1°C (Fig. 1), which are almost double the anomalies shown by F03 (due to the different composite years chosen by these authors).

Generally, the dipolelike anomalies commence in November of the onset year, peaking in February/March of the event year, and dissipate thereafter. This timing can vary between events, sometimes with the dipole pattern not totally diminishing (1981/82 positive event and 1949/50 negative event) and sometimes reversing poles (1950/51 and 1975/76 events). To investigate the evolution, monthly composites of the onset, event, and subsequent years were created from the model SST (see Table 1) and the model months corresponding to the austral summer for both the positive and negative events are shown in Fig. 3.

For the positive event, Figs. 2 and 3a,b show that the dipole pattern commences in both oceans toward the end of the onset year, preceding the event. The South Atlantic dipole peaks in months 1–2 and the South Indian Ocean dipole in months 2–3 of the following year, that is, the event year (Figs. 3c–e). The approximately 1-month lead of the South Atlantic over the South Indian Ocean suggests a westerly propagating atmospheric forcing pattern, and this is discussed further in section 4. The negative anomaly has weakened by month 5 of the positive event year in the South Indian Ocean, but the warm pole exists until month 9 of the event year (not shown). Both poles are apparent in the South Atlantic Ocean until month 9. In both oceans, both poles are strongest during months 1–5 of the composite event years, although the warm pole moves eastward during its dissipation, possibly due to eastward migration of the atmospheric forcing by the mean westerly flow.

Prior to the evolution of the negative event, both oceans show warm anomalies over most of the area from the equator to 35°S (excluding the Agulhas Current and the Indonesian Throughflow area). During the negative event, the cool, western pole is larger in the model South Indian Ocean. Warm (cold) poles first become evident in month 13 of the negative event onset years in the east (west) of the South Indian and South Atlantic Oceans (Figs. 2b and 3f). The dipole appears to peak in months 2–3 in the South Atlantic Ocean and months 3–4 in the South Indian Ocean. In both oceans, there are signs of the anomalies until month 12 of the event years. During both positive and negative events, the spatial distribution of the anomalies is similar, although negative events appear to reach maturity about 1 month later than positive events.

Figure 3 shows that cyclonic (anticyclonic) wind anomalies occur over both oceans during a negative (positive) event. We suggest that negative events may take longer to peak and are less coherent than the positive events because they are related to a weakening or reversal of the summer southward shift and strength-

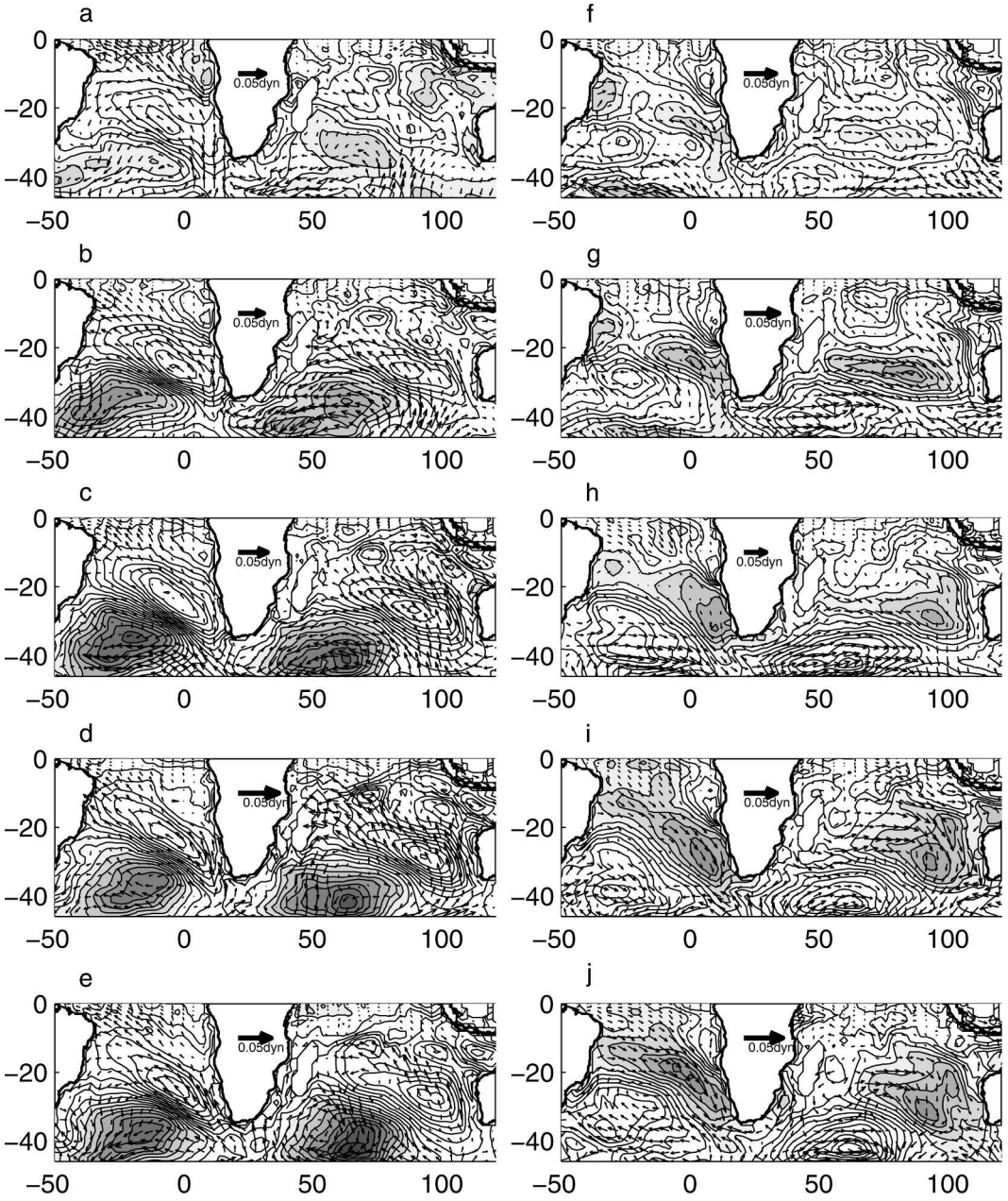

FIG. 3. (a)–(e) ORCA2 SST and wind stress anomalies for months 14 (onset year) through to month 3 of the event year for the positive dipole event. Contour interval is 0.05°C, positive (negative) values are shaded gray (white). A scale wind stress vector of 0.05 dynes cm^{-2} is shown. (f)–(j) Same as for (a)–(e) but for the negative event.

ening of the subtropical anticyclone. This process might be less stable and need a longer time to become established, since it opposes the annual cycle.

To examine the interannual variability of the dipole in the model, ORCA2 data were used to create an index. Similar to BY01 for the South Indian Ocean, the index is based on the SST anomaly difference between an area in the west (30°–44°S, 74°–44°E) and the east (19°–35°S, 80°–110°E). A similar method was used to create an index for the South Atlantic Ocean (44°–32°S, 38°–8°W in the west and 30°–18°S, 15°W–15°E in the east). Both model indices are smoothed by a 5-month running mean and compare well with those derived from GISST 2.3 data (not shown). In Fig. 4, the SIOD index is shown in black and the South Atlantic dipole (SAOD) index in gray. The years where dipoles occurred in both ba-

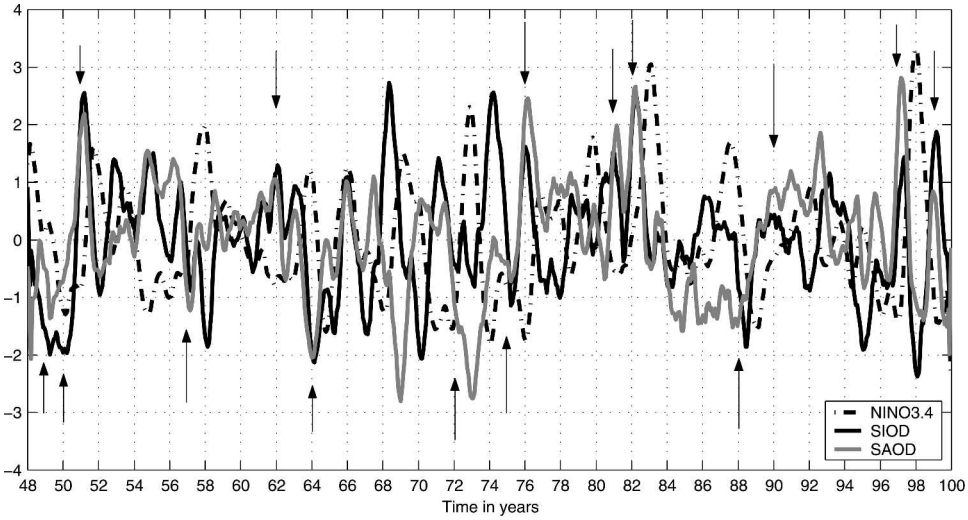

FIG. 4. Index for the Indian Ocean (black), the Atlantic Ocean (red), and ENSO3.4 (dashed). Data have been normalized using the standard deviation and smoothed by a 5-month running mean. The years where dipoles occurred in both basins have been marked by arrows (downward-pointing arrows mark positive events and upward, negative events).

sins have been marked by arrows (downward-pointing arrows mark positive events and upward, negative events).

Most of the time the South Indian series appears in phase with the South Atlantic, however, sometimes they are out of phase. There may be a decadal pulsing of this relationship—for example, good agreement between the two indices is apparent for 1950–55, the late 1970s–early 1980s, and 1994–99 but they appear out of phase in the late 1980s and 1968–71. The correlation between the two indices is 0.41, with the Atlantic leading by 1 month. However, from 1948 to 1967 the correlation increases to 0.74, with the South Atlantic Ocean leading by 2 months. From 1968 to 1976, the South Indian and South Atlantic Ocean indices are further out of phase (they are correlated at -0.4 with a 9-month lag). From 1978 to 1984 and from 1997 to 2000, there are zero lag correlations of 0.64 and 0.66, respectively, whereas in the intervening 1984–94 period the two indices appear less obviously related.

The problem with this type of index is that the dipole events can vary substantially in both position and strength, from event to event. Hence, it is important to understand that the strongest anomalies may not always occur in the specified area used to form the index. This is especially apparent in the slightly different positions chosen in this study compared with those used in BY01, because of the extra years used here. Because of this, a strong dipole may occur in both oceans but may not be visible in the index, and hence it is vital to examine the individual SST anomalies for each year in choosing the dipole events. In addition, a large index value can be apparent when there is just one very large anomaly in one of the boxes and little or no anomaly in the other. Although such time series are useful for revealing possible variability in the relationships through the record, as well as possible linkages with other large-scale modes such as ENSO, they must be viewed with caution. Furthermore, Fig. 4 and the raw data indicate that there are strong dipole events that occur in, for example, the South Indian Ocean and not in the South Atlantic. An example of this is 1968, when there was strong warming in the southwest Indian Ocean and cooling in the northeast, however, there was little evidence of a dipole in the South Atlantic.

Also shown as the dashed curve in Fig. 4 is the smoothed Niño-3.4 time series. Each time series was then filtered (using a 2–7-yr filter) and correlations were performed between the indices for each ocean with Niño-3.4. Niño-3.4 leads the South Atlantic Ocean by 2 model months, with a correlation of -0.43 and leads the South Indian Ocean by 5 model months, with a correlation of -0.42. Although BY01 did not consider relationships with ENSO and F03 suggest only a weak lead–lag relationship, Fig. 4 implies that there may well be a significant ENSO relationship. Similar correlations were also performed using smooth, filtered GISST data. Niño-3.4 was found to lead the South Indian (South Atlantic) Ocean by 6 (3) months, with a correlation of -0.49 (-0.64). These correlations are significant at the 99% confidence level, based on the method modified by Davis (1976). This may suggest that the

higher correlation found here than by BY01 and F03 can be explained partly by the use of the 2–7-yr filter and also by the different areas chosen to create the index. The fact that the Niño-3.4 index leads the South Atlantic index by fewer months than its lead over the South Indian index is consistent with the anomalies occurring in the South Atlantic Ocean prior to the South Indian Ocean. Such a phasing would be consistent with a Pacific–South America pattern in the atmospheric forcing driven by ENSO (e.g., Mo and White 1985; Mo and Paegle 2001) where the midlatitude western South Atlantic responds more quickly than the eastern, and the South Indian Ocean later still. If an index is created for both the South Atlantic and the South Indian Oceans combined (not shown), there is a correlation with Niño-3.4 of −0.50, lagging by 3 months.

Some, but not all, of the positive dipole years appear to occur during or after La Niña events and several of the negative dipole years occur during or after El Niño. This is not surprising given the dipolelike SST patterns observed in the Indian and South Atlantic Oceans in raw SST seasonal composite anomalies based on strong El Niño and La Niña events over the last century (Reason et al. 2000). When the two oceans are out of phase, the relationship between ENSO and the South Indian Ocean becomes reversed, but it remains the same with the South Atlantic Ocean. Dipole years also occur during non-ENSO years. In general, there is likely to be a complex interaction between the SST anomalies in the South Atlantic and South Indian Oceans and ENSO events. One possibility, which is beyond the scope of the current study but that should be investigated, is whether these two basins have a preference for forming dipolelike SST anomaly patterns and whether the associated atmospheric forcing (modulation of the subtropical anticyclones in each basin) is, in turn, driven by a variety of modes including ENSO.

4. Large-scale atmospheric forcing and the ocean response

To assess the potential atmospheric forcing, a composite of 500-hPa summer geopotential height anomalies was made for both the positive and negative events (Figs. 5a,b). A wavenumber-4-type pattern is visible in both cases. Individual months were examined (not shown) to show that during some months the anomaly over the southwest Pacific and Tasman Sea is joined, whereas in others, it is more clearly separated. During a positive event (Fig. 5a), high pressure anomalies are evident in the central South Atlantic, South Indian, and much of the South Pacific Ocean. These are also apparent at sea level pressure, similar to those derived by F03. The reverse is seen during a negative event (Fig. 5b), but the anomalies are stronger and display an (Antarctic Oscillation) AAO-type pattern with a superimposed wavenumber-4 feature in the midlatitudes. Since it is well known that the AAO has become more positive in phase since the 1980s (e.g., Mo 2000; Thompson and Wallace 2000), Fig. 5c shows the 500-hPa composite of positive events after 1980, which results in a more obvious AAO pattern. These results, combined with the fact that the positive (negative) events tend to be more frequent later (earlier) in the 1948–99 period, suggests that there may be a link between the AAO and the dipole events.

Although the results are generally in agreement with F03, some differences should be emphasized. First, the anomalies in sea level pressure and 500-hPa height tend to be stronger here than in F03 and maintain their magnitude throughout the November/February period (F03 found larger anomalies in early than in late summer). Second, both the SST and 500-hPa anomalies appear to be centered at higher latitudes than those of F03, consistent with the suggestion that midlatitude atmospheric forcing is important in their evolution.

In addition, the AAO patterns apparent in Fig. 5 are less evident in the composites shown in F03. In choosing their composites, these authors only included years with a warm anomaly in the southwest Indian and Atlantic Oceans, whereas, our study also requires a simultaneous cool anomaly on the other side of each basin. Thus, the relationship between the AAO and the anomalous SST dipole patterns may be strongest when there is both a clearly defined and strong warm and cool pole. Furthermore, F03 chose composite (positive dipole) years that consisted of more years pre-1980 and less afterward (i.e., when the AAO tended to be in a more negative phase).

Associated with the anomalies in 500-hPa geopotential heights, shown in Fig. 5, the corresponding anticyclones over the South Indian and South Atlantic Oceans are strengthened (and shift southward) during the positive events (Figs. 3a–c and 5a). This shift is superimposed on the seasonal southward shift of the subtropical highs that occurs in summer. During the positive events, the stronger anticyclones lead to increased southeasterlies west of Australia and southern Africa (Figs. 6a,b), causing increased evaporation and upper-ocean mixing, lowering SST in this region.

During the positive events, the southeasterly anomalies in the South Atlantic (Figs. 6a,b) are stronger in October–November–December (OND) than JFM, consistent with the cold anomaly arising there first. This increase in winds leads to an increase in offshore Ekman transport and coastal upwelling in the northern

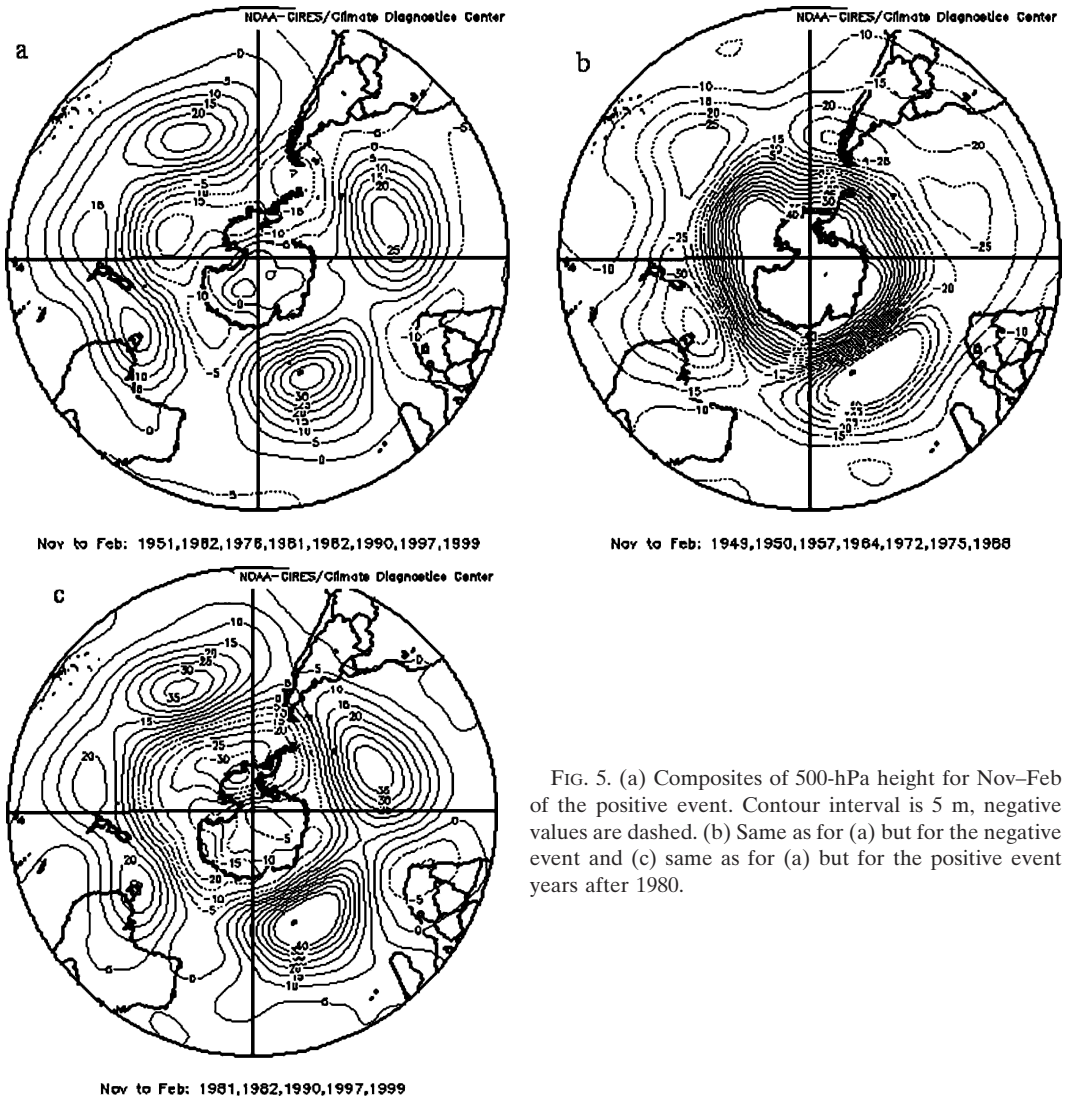

FIG. 5. (a) Composites of 500-hPa height for Nov–Feb of the positive event. Contour interval is 5 m, negative values are dashed. (b) Same as for (a) but for the negative event and (c) same as for (a) but for the positive event years after 1980.

and southern Benguela region, and hence cooling inshore as well as offshore. Farther to the southwest over the central midlatitudes, a weakening of the westerlies is apparent, helping to warm the ocean in the western part of each basin. South of 35°S, over the warm pole in both oceans, the westerlies are decreased, implying reduced evaporation and upper-ocean mixing and hence warming, as well as less equatorward Ekman drift of cooler waters from the south.

During the negative events, the low pressure anomaly over the midlatitude South Indian Ocean is particularly strong, with significant cyclonic features also present over the midlatitude South Atlantic Ocean, the Tasman Sea, and the South Pacific Ocean (Fig. 5b). The South Indian anomaly is stronger than the high pressure anomaly during the positive event and the composite as a whole has a stronger AAO signal. The cyclonic anomalies are centered in roughly the same positions as the anticyclonic features during the positive events. The climatological southerlies off the coast of Western Australia and southwestern Africa are weakened during the negative events by the cyclonic anomalies in the South Indian and South Atlantic Oceans (Figs. 6c,d). As a result, decreased upper-ocean mixing and surface evaporation is expected, leading to the warm pole over the southeast Indian and Atlantic Oceans. The climatological westerlies over the central and western midlatitudes of the South Indian and South Atlantic Oceans are increased during the negative event in JFM, and to lesser extent OND, implying increased evaporation and upper-ocean mixing there and hence leading to the cool pole. The cyclonic anomalies

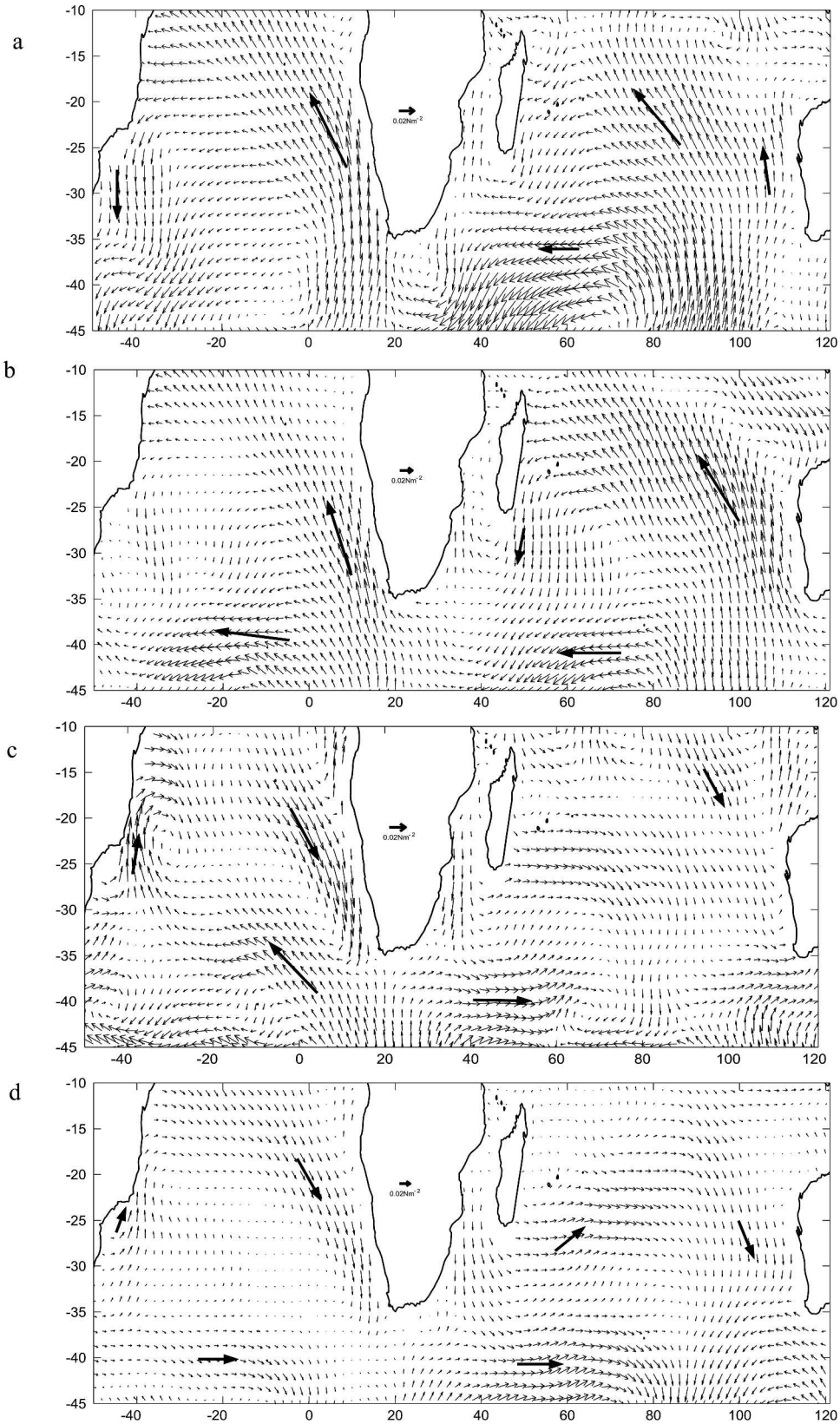

FIG. 6. (a) Wind stress anomalies of the positive event for OND. A scale wind stress vector of 0.02 N m^{-2} is shown. (b) Same as (a), but for JFM of the positive event. (c), (d) Same as for (a), (b), respectively, but for the negative event.

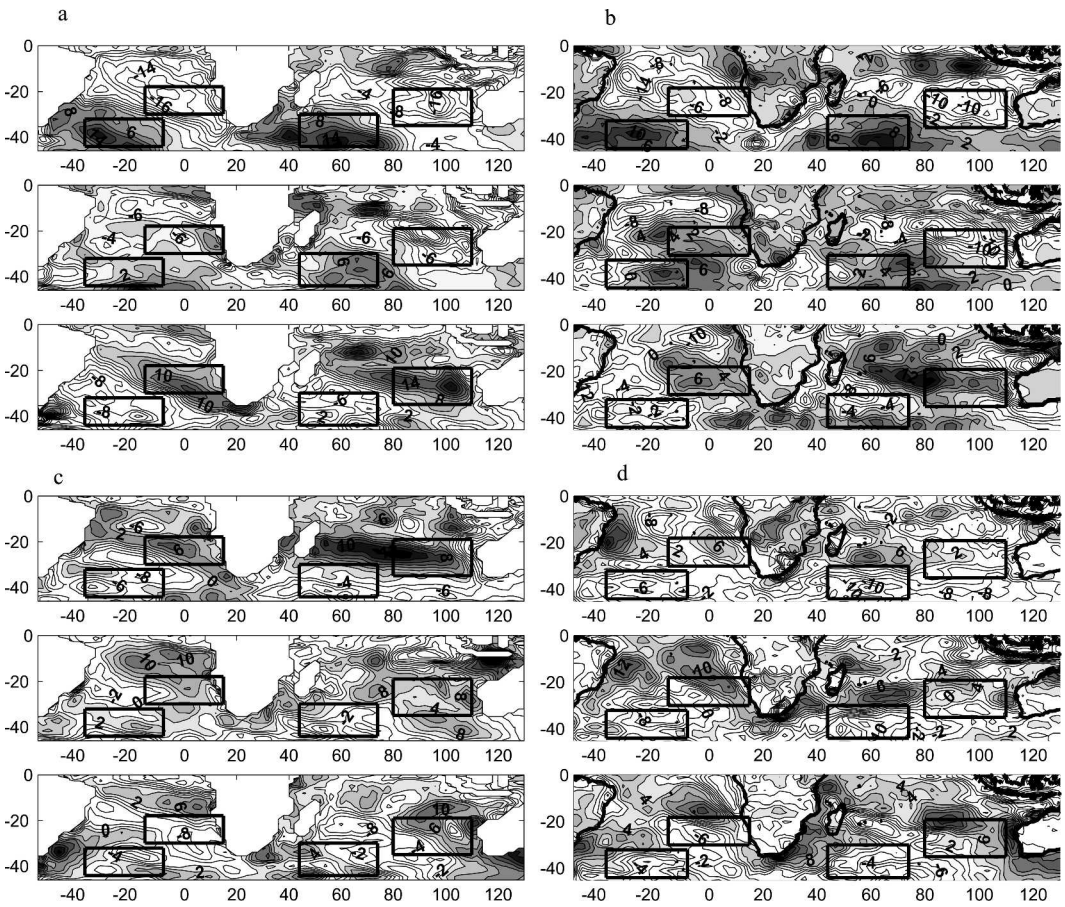

FIG. 7. (a) Heat flux anomalies for the positive event, OND, JFM, and AMJ. Contour interval is 2 W m^{-2}, positive (negative) values are shaded gray (white). (b) Same as (a), but for NCEP latent heat flux. (c), (d) Same as (a), (b), respectively, but for the negative event.

in this region also suggest upwelling over the southern part of the cold pole in the southwest Indian and Atlantic Oceans.

Figures 5–6 suggest that the SST dipole events are forced by these large-scale modulations of the atmospheric circulation. The highest correlation values (0.4) between the 500-hPa geopotential height and the South Indian and South Atlantic dipole indexes were achieved when the geopotential height leads the index by 1 month. To investigate this atmospheric forcing of the ocean in more detail, the next section examines the surface heat fluxes.

5. Surface heat fluxes

The ORCA2 net seasonal downward heat flux anomaly for the positive and negative events is shown in Figs. 7a and 7c, respectively, where the boxes mark the position of the strongest SST anomalies during the composite years and a negative value represents increased heat loss to the atmosphere. There is not much variation in heat flux within each individual season, thus the figures shown are for the austral spring (OND) of the onset year, summer (JFM), and autumn [April–May–June (AMJ)] of the event years.

During onset of the positive event in OND, there is a "dipole" pattern in the surface heat flux anomalies, which subsequently weakens the following summer (JFM) and then reverses in sign in AMJ (Fig. 7a). The OND pattern shows heat loss to the atmosphere over the cold pole and heat gain over the warm. This implies that the atmosphere is forcing the ocean since the strongest fluxes occur during onset and weaken prior to the largest SST anomalies in JFM. By AMJ, the positive and negative heat flux poles switch sign and there is heat gain to the ocean over the cold SST pole and heat loss over the warm SST pole, acting to dampen the dipole pattern. The heat flux forcing from the atmosphere is directly tied to the shift in position and intensity of the high pressure anomalies over these oceans in

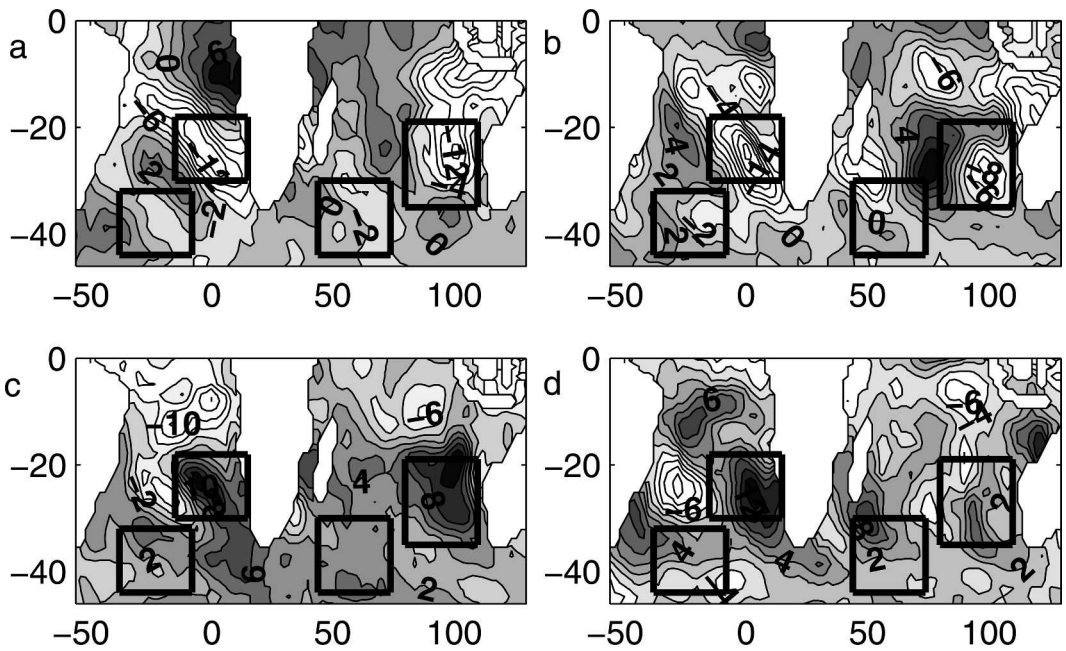

FIG. 8. (a) Shortwave radiation anomalies for the positive event, OND. Contour interval is W m^{-2}, positive (negative) values are shaded gray (white). (b), Same as (a), but for JFM of the positive event. (c), (d) Same as (a), (b), respectively, but for the negative event.

OND, modifying the climatological winds and SST. These anomalies shift farther southeast in JFM modulating the ocean response in AMJ.

During a negative dipole event, the heat flux anomaly is not quite as well defined, especially over the South Atlantic Ocean. In both oceans, there are areas of heat gain over the warm pole in the east and heat loss over the cold pole during OND, and JFM (Fig. 7c). The flux anomalies are not as strong or as coherent as those evident during a positive event, especially over the western pole of each basin. The heat gain over the eastern pole persists through JFM in the South Indian Ocean and strengthens over the South Atlantic eastern pole. This is because the negative dipole events seem to evolve later than the positive, so the heat flux anomalies are strongest over NDJ. During both events, the switch in sign of the heat flux anomalies seems to occur in the South Atlantic before the South Indian Ocean.

Figures 7b,d show the NCEP–NCAR latent heat flux anomalies for both positive and negative events (the sign has been reversed for comparison). ORCA model latent fluxes were not available but since the model is forced by NCEP–NCAR reanalyses, the NCEP–NCAR latent heat fluxes are likely to be a good approximation. The NCEP–NCAR heat fluxes cannot be directly compared to the SST but the figures suggest that, consistent with BY01, the latent heat flux anomalies make a significant contribution in the surface heat flux forcing of the SST anomalies.

Change in insolation may also lead to significant SST anomalies and Fig. 8 shows anomalies in this field during the events. Reduced insolation is observed over the cold pole leading up to, and during, a positive event, with an increase over part of the warm pole in OND and JFM (Figs. 8a,b). However, in both oceans it is the decrease in insolation over the cold pole, which is more coherent. The reverse is seen during negative events (Figs. 8c,d), again with the eastern pole (in this case the warm pole) having the stronger signal in (increased) insolation.

During the positive event, the high pressure is shifted south and strengthened. To the south of the cold pole, in the eastern part of the basins, increased southerly anomalies (Figs. 6a,b) lead to enhanced advection of cool, moist, marine air from the midlatitudes, which is favorable for an increase in stratus cloud cover and a decrease in shortwave radiation (SWR) received at the surface. During the negative event, the high pressure is weakened but also moves east, so there are northwesterly anomalies over the eastern (warm) pole in OND, reducing the influx of cooler marine air and hence the cloud cover. These results suggest that changes in cloud cover can also play a role in the evolution of these events in both the South Atlantic and South Indian Oceans, particularly over the eastern part of each basin.

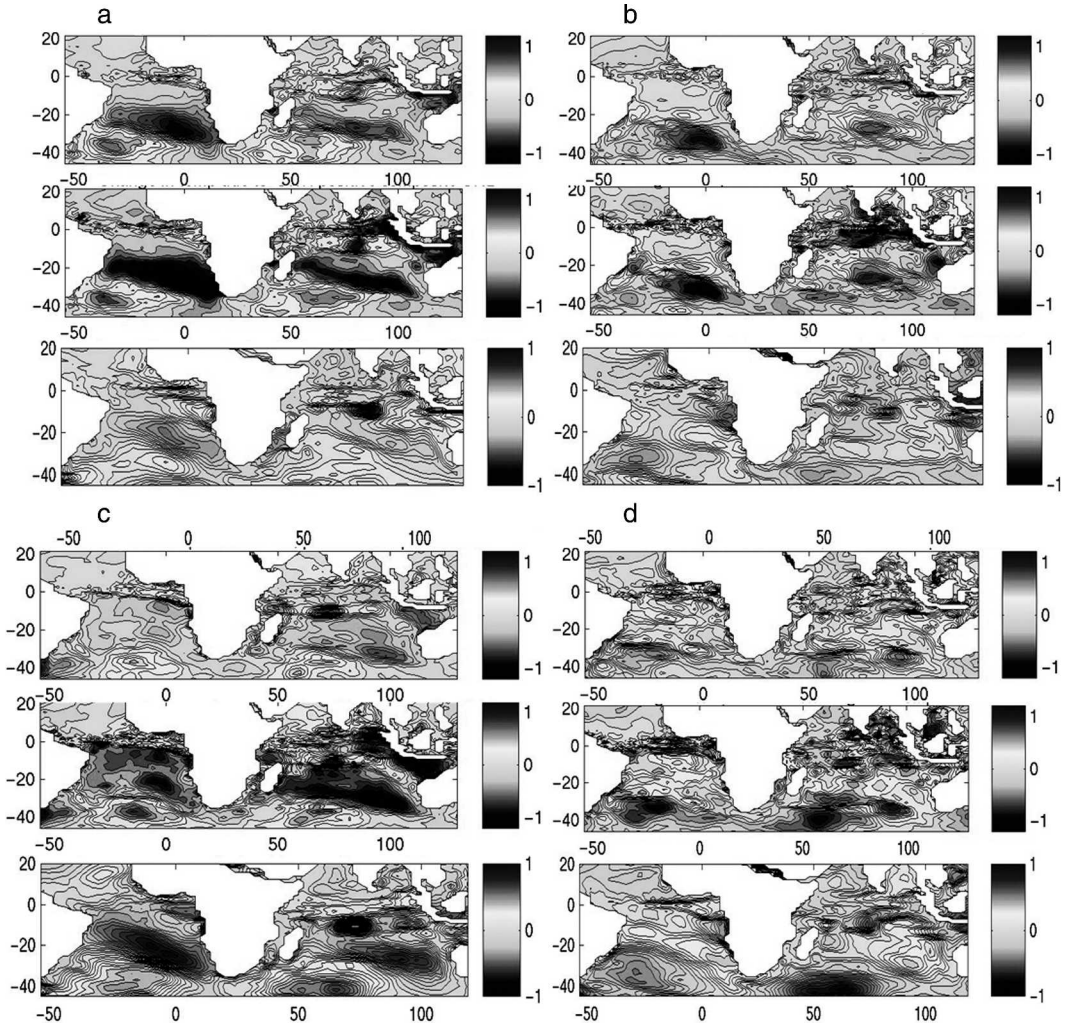

FIG. 9. (a) Calculated change in temperature due to surface heat flux and shortwave radiation for OND of the positive event and actual temperature of upper model 50 m for OND of the positive event. Contour range is −1.2° to 1.2°C, contour interval is 0.05°C. (b) Same as (a), but for the negative event. (c), (d) Same as (a), (b), respectively, but for JFM.

To further examine whether changes in the surface heat flux (or SWR) are consistent with the SST anomalies, the expected temperature change from each variable has been calculated as follows (note that possible influences from advection and entrainment have not been included):

$$\frac{dT}{dt} = \frac{\text{HFL}}{\text{Cp} \times \rho \times h}$$

HFL = Heat flux (W m^{-2}) (or SWR),

h = Depth of the mixed layer, diagnosed from model (m),

Cp = Specific heat capacity (4187 J kg^{-1} K^{-1}),

ρ = Density of seawater (1027 k gm^{-3}), and

T = Temperature (K).

Figure 9 shows the predicted temperature of the mixed layer from the surface heat flux, from just the SWR flux and, finally, the model change in temperature averaged over the upper 50 m during OND and JFM for both the positive and negative events. These figures indicate that the surface heat flux exchange with the atmosphere plays a large part in forming the anomalous temperature patterns. Since the SWR contributes to the surface heat flux, Fig. 9 suggests that the other terms in the heat budget counteract its effect to some extent. The predicted temperature pattern compares well in position and strength (agreeing best with a 1-month lag;

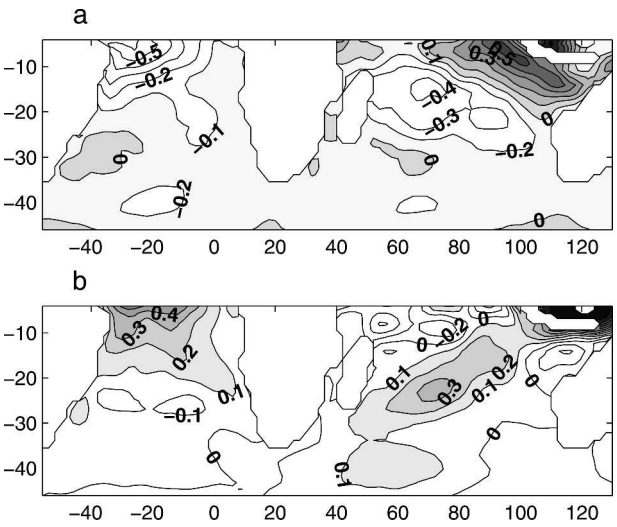

FIG. 10. (a) Meridional Ekman heat transport ($\times 10^8$) for JFM of the positive event. Contour interval is 2×10^7 W m^{-1}, positive (negative) values are shaded gray (white). (b) Same as for (a), but for the negative event.

not shown) with the averaged upper 50-m temperature. However, after the peak in JFM, the predicted SST weakens faster than the actual temperature and by month 4, there is a weak reversal in the temperature tendency. The predicted temperature change due to the surface heat flux is considerably (slightly) stronger in OND than JFM during the positive (negative) events, consistent with the negative event commencing later than the positive event.

6. Ekman heat fluxes

Another possible mechanism that could influence SST is meridional Ekman heat transport. To investigate this possibility, we have computed the Ekman heat transport as per Levitus (1987). In both the South Indian and South Atlantic Oceans, there is generally a poleward Ekman heat transport. However, during a positive event there is a positive anomaly in the northeast of the South Indian Ocean (Fig. 10). This implies a reduction of the climatological southward heat transport over the eastern part of the basin; thus, there is less heat being transported than average toward the area of the cold pole, helping to cool this region. In the west of this basin, the heat transport anomaly is negative, suggesting an increase in poleward heat transport toward the area of the warm pole.

During the negative event, there is a decrease in the southward climatological heat transport toward the southwest of the basin (cool pole) and an increase in heat transport toward the warm pole. These patterns have the most coherent signal during JFM, when the heat exchange with the atmosphere is not as significant (Figs. 7–9), suggesting that anomalies in the Ekman heat transport help to maintain the SST poles in the South Indian Ocean. In the South Atlantic Ocean, the meridional Ekman heat transports anomalies are mainly negative (positive) during the positive (negative) dipole events and are strongest toward the west of the basin. This implies an increase (decrease) in southward heat transport toward the warm (cool) pole in the SW. There is little evidence of a decrease (increase) in this transport near the eastern pole during the positive (negative) event.

The anomalous winds described earlier also influence the currents in the South Atlantic and South Indian Oceans. During OND of the onset year of the positive (negative) event (not shown) and JFM of the positive (negative) event year (Fig. 11), there are westward (eastward) current anomalies, between 15° and 20°S, strengthening (weakening) the South Equatorial Current in the South Indian Ocean. There is a 20% increase (8% decrease) in the westward heat transport in the upper 100 m (JFM model climatology is 1.24 PW) in this region during the positive (negative) events. Figures 11a,b suggest changes in the advection of warmer tropical water westward, which, via the enhanced (reduced) East Madagascar and Agulhas Currents, may contribute toward the western pole. These changes correspond to a 13% increase of the 0.33 PW JFM climatological southward heat transport in the Agulhas Current during the positive events and an 18% decrease during the negative.

The current anomalies in the South Atlantic are weaker but may still lead to some changes in heat advection by the Brazil Current that could influence the western pole. There is a 7% increase in southward heat transport in the Brazil Current during a positive event and a decrease of up to 12% of the 0.56 PW climatological heat transport during the negative event. Farther south, the weakened (strengthened) Falklands/Malvinas Current reduces (increases) the mean northward transport of cold water toward the warm (cool) western pole during the positive (negative) event.

During the positive (negative) event, there are anomalous westward (eastward) current anomalies in the southeastern Indian Ocean, thus weakening (strengthening) the geostrophic inflow toward the Leeuwin Current (Godfrey 1996) and cooling (warming) the ocean near the eastern pole. In the South Atlantic, a strengthening (weakening) of the southern Benguela Current occurs during the positive (negative) event, increasing (reducing) the cool water heading toward the region of the cool (warm) pole. Offshore of

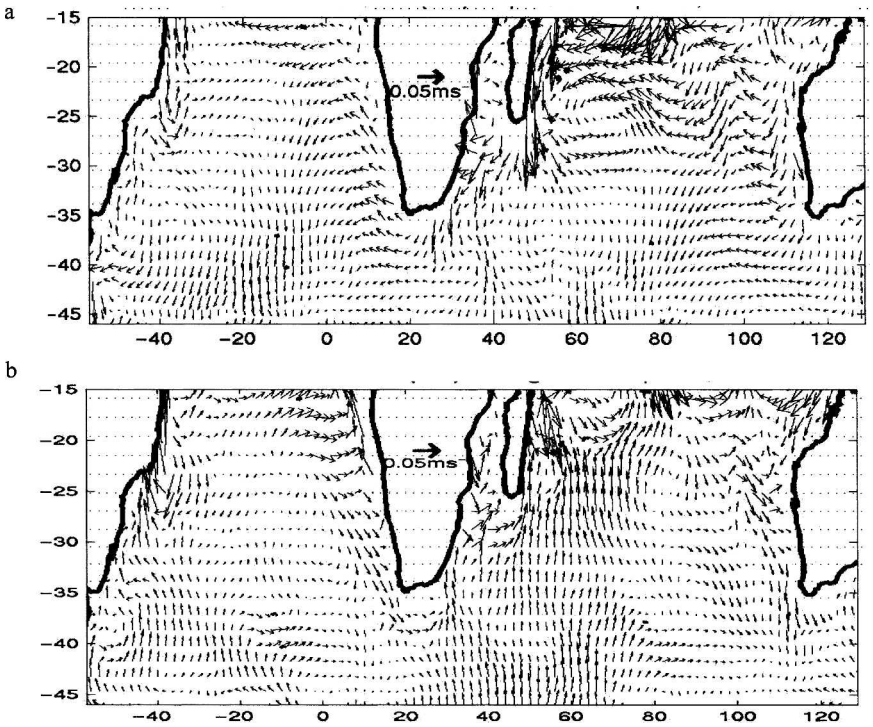

FIG. 11. (a) The U and V current anomalies for JFM of the positive event. A scale current vector of 0.05 m s^{-1} is shown. (b) Same as for (a), but for the negative event.

the western boundary currents, strong southward (northward) current anomalies are apparent in the southwest Indian and Atlantic Oceans during the positive (negative) event, implying a decrease (increase) in colder water being advected northward toward the warm (cool) pole. These anomalies represent a 20% change in the mean southward heat transport of 0.16 PW in the upper 100 m of the South Indian Ocean and between a 40% and 50% change in the mean heat transport of 0.05 PW in the South Atlantic Ocean.

The wind stress curl (Figs. 12a,c) in the northeast of each basin (which is climatologically negative) shows negative (positive) anomalies during the positive (negative) dipole event. This would imply a strengthening (weakening) of the subtropical gyre of each basin during the positive (negative) event. However, in the southwest of the South Atlantic and South Indian Oceans, the climatologically positive wind stress curl is decreased (increased) during the positive (negative) event. This corresponds with the decrease (increase) in the westerlies here and hence implies a decrease (increase) in the Ekman transport of colder, midlatitude water advected toward the warm (cool) pole.

Ekman pumping was also investigated (not shown). Areas of downwelling were found over some regions of the warm pole during the events and upwelling over some areas of the cold pole. Increased upwelling (downwelling) was evident during the positive (negative) event over the cold (warm) pole in the southeast Indian and Atlantic Oceans, especially off the west coasts of Australia and South Africa/Namibia, due to the increased (decreased) southeasterlies evident there in Fig. 6. During positive (negative) events, down-

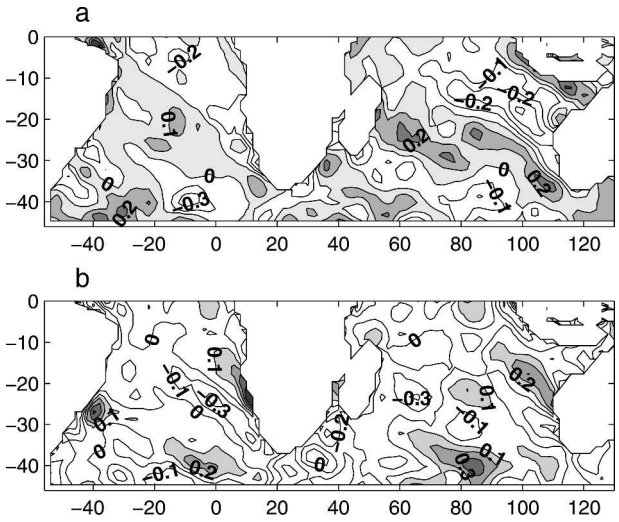

FIG. 12. (a) Wind stress curl anomalies ($\times 10^8$) for JFM of the positive event. Contour interval is 0.1×10^8 kg s^{-2} m^{-2}. (b) Same as for (a) but for the negative event.

TABLE 3. Forcing mechanisms contributing to each anomaly pole and their duration. Numbers refer to the start and finishing months of the onset and event years.

	Positive dipole			
	SW Indian Ocean	SW Atlantic Ocean	SE Indian Ocean	SE Atlantic Ocean
SST	12–9	13–9	12–6	12–9
Mechanism	Model months (12–15 refers to onset yr, 1–11 refers to event yr unless stated otherwise)			
Heat flux	10–1	10–1	10–1	10–1
SWR	15–2	15–2	11–2	11–2
Upwelling	12–13, 15–3	12–13, 15–2	12–13, 15–3	12–13, 15–2
Ekman HFL	14–3	14–3	14–4	—
	Negative dipole			
	SW Indian Ocean	SW Atlantic Ocean	SE Indian Ocean	SE Atlantic Ocean
SST	14–12 (event yr)	12–12 (event yr)	14–12 (event yr)	12–12 (event yr unless stated otherwise)
Mechanism	Model months (12–15 refers to onset yr, 1:11 refers to event yr)			
Heat flux	14–2	14–2	14–2	14–2
SWR	15–1	15–4	12–1	11–5
Upwelling	14–3	13–3	14–3	13–3
Ekman HFL	1–3	12–5	1–3	—

welling (upwelling) is evident off southeast Brazil, where the northward and southward current anomalies converge (diverge) in Fig. 11 and this helps contribute to the warm (cool) pole.

A summary of the timing and location of the major mechanisms is shown in Table 3. Upwelling (not shown) seems to play a significant role in the formation of the cool poles, and is more persistent during the negative event. During the positive event, modulations to the upwelling relax between months 13 and 15 of the onset year. Surface heat flux exchange with the atmosphere seems to be the most coherent forcing mechanism, persisting for 7 (4) model months over each pole in both oceans during the positive (negative) events.

7. Rossby waves

The significance of Rossby waves for interannual SST variability in the South Indian Ocean has been examined by Xie et al. (2002). Figures 13a,b show Hovmöller plots of the sea surface height (SSH) anomalies at 20°S for the onset and event composite years. During the positive (negative) event, an upwelling (downwelling) wave starts at 100°E in month 7 and travels westward at around 8 km day^{-1} (approximate speed of a Rossby wave at 20°S). A downwelling (upwelling) wave is evident to the east of the strong features at around 110°E during the positive (negative) event. The waves are most intense during the end of the onset year and the beginning of the event year. Some evidence of a Rossby wave signal can be seen in the South Atlantic, but it is much weaker than that in the South Indian Ocean. Similar upwelling/downwelling Rossby waves were also seen at 10°S (not shown). These Rossby waves may influence upper-ocean heat content in the source regions of the western boundary currents and hence the evolution of the western pole. The 10° and 20°S zones in the South Indian Ocean have been previously described as having high Rossby wave variability (Xie et al. 2002; Schouten et al. 2002). Xie et al. (2002) proposed a correlation between SST off Sumatra and SST in the subtropical southeastern Indian Ocean, with modulations of the trade winds off Sumatra leading to changes in upwelling, and hence SST there, as well as exciting Rossby waves that propagate the SST and thermocline signal to the subtropical western part of the basin. They found the variability to be locked to the seasonal cycle, growing rapidly from September to November at 82°E. Figure 6 shows modulations of the trades off Sumatra/northwest shelf region of Australia during the positive event and, to a lesser extent, in the negative event consistent with the stronger Rossby wave signal during the former. Consistent with the generally weaker modulations to the winds in the tropical southeast Atlantic, there is less evidence of Rossby wave signals in this basin.

8. Summary and conclusions

This study has used a global ocean model (ORCA2) driven with 52 yr of NCEP–NCAR reanalysis winds

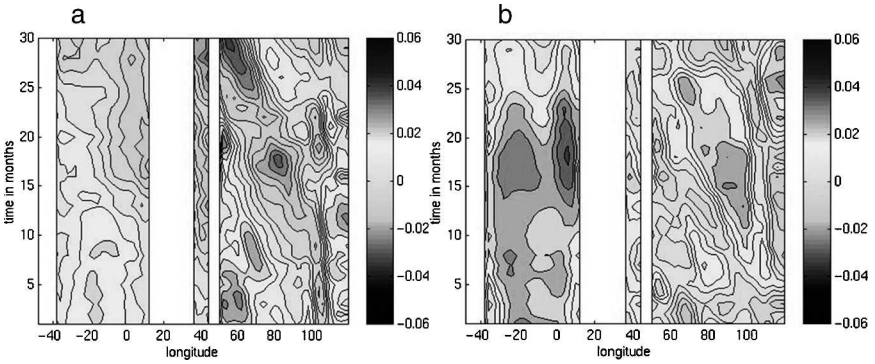

FIG. 13. (a) Time–longitude section SSH anomalies for the positive event (onset through to event years) at 20°S. Contour range is −0.06 to 0.06 m, contour interval is 0.005 m. (b) Same as for (a), but for the negative event.

and fluxes to investigate the forcing processes associated with austral summer SST dipole events in the South Atlantic and South Indian Oceans. A positive (negative) event occurs when there are warm (cool) SST anomalies in the southwest (northeast) of the South Atlantic and South Indian Oceans.

Large-scale atmospheric modulation of the midlatitude Southern Hemisphere circulation (wavenumber-4 and Antarctic Oscillation–type patterns) plays a role in the formation of both the positive and negative events. As a result, the events are highly correlated between the two oceans due to this coherent large-scale forcing. These atmospheric patterns lead to modulations of the trades and westerlies over each basin, which then influence SST in various ways. During some years (e.g., 1968), the atmospheric circulation anomalies are much stronger in the South Indian Ocean and there is less evidence of a coherent wavenumber-4 pattern or Antarctic Oscillation feature, leading to dipolelike SST anomalies only in this basin and not in the South Atlantic. Individual events occurring in either one of the two oceans only were examined and, for both the negative and positive events, hemispheric-scale atmospheric anomalies were absent or less prominent than for the cases considered here.

As a result it appears that both the South Atlantic and the South Indian Ocean are prone to display dipolelike SST anomalies if the semipermanent anticyclone in the basin is sufficiently modulated; however, for both basins to show these SST patterns there needs to be a near-hemispheric modulation of the subtropical anticyclones and circumpolar trough. As suggested by Fig. 4 and the various correlations with the Niño-3.4 index, there appears to be a relationship between the events and ENSO. Given that ENSO projects onto the subtropical to high-latitude atmospheric circulation of the South Atlantic and farther east via the Pacific–South America pattern (Mo and White 1985; Mo and Paegle 2001), this linkage is not surprising.

Locally over each basin, the modulations to the anticyclonic circulation lead to changes in the net surface heat flux, Ekman heat transports, and up- and downwelling, which contribute toward the generation and evolution of the warm and cold poles. Some contribution of advection via modulated equatorial and western boundary currents is also evident in both basins, more so in the southwest Indian Ocean than in the southwest Atlantic Ocean. In addition, in the South Indian Ocean, strong Rossby wave signals are observed in the model during both the positive and negative events but there is less evidence of such activity in the South Atlantic.

The negative events appear strongly linked to the Antarctic Oscillation however, the forcing mechanisms appear less coherent for these events than for the positive events. Negative events take longer to become established when compared with positive events. We suggest this may be because negative events arise due to a weakening of the climatological winds over the South Atlantic and the South Indian Oceans, that is, opposing the annual cycle whereas the positive events, effectively act in the same sense as the annual cycle with a strengthening and southward shift of the anticyclones.

In terms of the nonlinearity between the negative and positive events, Figs. 1–6 show that, although the events have a similar spatial pattern, model positive event SST anomalies are stronger and more coherent than the negative. The positive events peak more quickly and die out more quickly than do the negative events and the forcing mechanisms are generally more coherent than during the negative events. Different forcing mechanisms appear to be stronger for the eastern pole than for the western pole, regardless of the polarity of the dipole pattern itself. For example, it can be seen from Figs. 8 and 10 and Table 3 that the SWR

is more significant in modulating the temperature in the east of the South Atlantic and South Indian Oceans, whereas the meridional Ekman transport seems to play a more important role in the west of the basins.

A wavenumber-4-type pattern is more defined in the positive events, whereas the negative events show a more obvious Antarctic Oscillation pattern, which could explain why the forcing mechanisms are not so clear in each basin for the negative events. It is also possible that the lack of coherency during the composite negative event may result from a greater variation between each negative event than is the case for the positive events.

The question remains as to whether the South Indian and South Atlantic Oceans preferentially respond to large-scale midlatitude atmospheric forcing to yield dipolelike patterns in SST, perhaps because of their spatial scales and the land–sea distributions in the region. The details of how large-scale modes such as ENSO and the Antarctic Oscillation project onto this atmospheric forcing and hence the Southern Hemisphere oceans needs further study. However, modulations to the semipermanent anticyclones in each basin and associated surface heat flux changes clearly appear to be fundamental in driving the SST variability, both in the observational analyses of Behera and Yamagata (2001) for the Indian Ocean events and Fauchereau et al. (2003) as well as the ocean model response examined herein.

Acknowledgments. Some funding was received from the South African Water Research Commission. We are grateful to Keith Rogers, Sabrina Speich, and Frank Colberg for supplying and help with the model data and for the useful comments from two anonymous reviewers.

REFERENCES

Behera, S., and T. Yamagata, 2001: Subtropical SST dipole events in the southern Indian Ocean. *Geophys. Res. Lett.,* **28,** 327–330.

Davis, R. E., 1976: Predictability of sea surface temperature and sea level pressure anomalies over the North Pacific Ocean. *J. Phys. Oceanogr.,* **6,** 249–266.

Fauchereau, N., S. Trzaska, Y. Richard, P. Roucou, and P. Camberlin, 2003: Sea surface temperature co-variability in the Southern Atlantic and Indian Oceans and its connections with the atmospheric circulation in the Southern Hemisphere. *Int. J. Climatol.,* **23,** 663–677.

Fichefet, T., and M. A. Morales Maqueda, 1997: Sensitivity of a global sea ice model to the treatment of ice thermodynamics and dynamics. *J. Geophys. Res.,* **102,** 12 609–12 646.

Godfrey, J. S., 1996: The effect of the Indonesian throughflow on ocean circulation and heat exchange with the atmosphere: A review. *J. Geophys. Res.,* **101** (C5), 12 217–12 237.

Kalnay, E., and Coauthors, 1996: The NCEP/NCAR 40-Year Reanalysis Project. *Bull. Amer. Meteor. Soc.,* **77,** 437–471.

Levitus, S., 1987: Zonally integrated meridional Ekman heat fluxes for the world ocean and individual ocean basins. *J. Phys. Oceanogr.,* **17,** 1484–1492.

——, and Coauthors, 1998: *Introduction.* Vol. 1, *World Ocean Database 1998,* NOAA Atlas NESDIS 18, 346 pp.

Madec, G., P. Delecluse, M. Imbard, and C. Lévy, 1998: OPA 8.1 Ocean General Circulation Model reference manual. Notes du Pôle de Modélisation de l'Institut Pierre-Simon Laplace, 11, 91 pp. [Available from LODYC, Université Pierrre et Marie Curie, Case 100, 4 place Jussieu, 75252 Paris Cedex 05, France.]

Mason, S. J., 1995: Sea-surface temperature—South African rainfall associations, 1910–1989. *Int. J. Climatol.,* **15,** 119–135.

Mo, K. C., 2000: Relationships between low-frequency variability in the Southern Hemisphere and sea surface temperature anomalies. *J. Climate,* **13,** 3599–3610.

——, and G. H. White, 1985: Teleconnections in the Southern Hemisphere. *Mon. Wea. Rev.,* **113,** 22–37.

——, and J. N. Paegle, 2001: The Pacific-South American modes and their downstream effects. *Int. J. Climatol.,* **21,** 1211–1229.

Morales Maqueda, M., 1995: Un modelo acoplado del hielo de mar y del oceano superficial para estudios climaticos. Ph.D. thesis, Universidad Complutense, Madrid, Spain, 426 pp.

Qian, W., H. Hu, Y. Deng, and J. Tian, 2002: Signals of interannual and interdecadal variability of air-sea interaction in the basin-wide Indian Ocean. *Atmos.–Ocean,* **40,** 293–311.

Rayner, N. A., E. B. Horton, D. E. Parker, C. K. Folland, and R. B. Hackett, 1996: Version 2.2 of the global sea-ice and sea surface temperature data set, 1903–1994. Climate Research Tech. Note 74, Met Office, Bracknell, United Kingdom.

Reason, C. J. C., 1999: Interannual warm and cool events in the subtropical/mid-latitude south Indian Ocean region. *Geophys. Res. Lett.,* **26,** 215–218.

——, 2001: Subtropical Indian Ocean SST dipole events and southern African rainfall. *Geophys. Res. Lett.,* **28,** 2225–2227.

——, 2002: Sensitivity of the southern African circulation to dipole sea-surface temperature patterns in the South Indian Ocean. *Int. J. Climatol.,* **22,** 377–393.

——, and H. Mulenga, 1999: Relationships between South African rainfall and SST anomalies in the Southwest Indian Ocean. *Int. J. Climatol.,* **19,** 1651–1673.

——, R. J. Allan, J. A. Lindesay, and T. J. Ansell, 2000: ENSO and climatic signals across the Indian Ocean Basin in the global context. Part I: Interannual composite patterns. *Int. J.Climatol.,* **20,** 1285–1327.

Rodgers, K., B. Blanke, G. Madec, O. Aumont, P. Ciais, and J.-C. Dutay, 2003: Extratropical sources of equatorial Pacific upwelling in an OGCM. *Geophys. Res. Lett.,* **30,** 1084, doi:10.1029/2002GL016003.

Schouten, M. W., W. P. M. De Ruijter, P. J. Van Leeuwen, and H. A. Dijkstra, 2002: An oceanic teleconnection between the equatorial and southern Indian Ocean. *Geophys. Res. Lett.,* **29,** 1812, doi:10.1029/2001GL014542.

Smith, W. H. F., and D. T. Sandwell, 1997: Global sea floor topography from satellite altimetry and depth soundings. *Science,* **277,** 1956–1962.

Suzuki, R., S. K. Behera, S. Iizuka, and T. Yamagata, 2004: Indian

Ocean subtropical dipole simulated using a coupled general circulation model. *J. Geophys. Res.,* **109,** C09001, doi:10.1029/2003JC001974.

Thompson, D. W. J., and J. M. Wallace, 2000: Annular modes in the extratropical circulation. Part II: Trends. *J. Climate,* **13,** 1018–1035.

Venegas, S. A., L. A. Mysak, and D. N. Straub, 1997: Atmosphere-ocean coupled variability in the South Atlantic. *J. Climate,* **10,** 2904–2920.

Walker, N. D., 1990: Links between South African summer rainfall and temperature variability of the Agulhas and Benguela current systems. *J. Geophys. Res.,* **95,** 3297–3319.

——, and R. D. Mey, 1988: Ocean/atmosphere heat fluxes within the Agulhas retroflection region. *J. Geophys. Res.,* **93** (C12), 15 473–15 483.

Xie, S.-P., H. Annamalai, F. A. Schott, and J. P. McCreary, 2002: Structure and mechanisms of South Indian Ocean climate variability. *J. Climate,* **15,** 864–878.